Evaluating the effects of subsoiler type and spacing on tillage resistance and soil conservation with DEM simulation and field experiment

Yueming Wang[1], Chenjie Lu[1], Jiajun Fan[1], Xu Zhang[2,3], Kai Chen[4], Jing Chen[2,3*], Xiaoguang Li[5*]

(1. *School of Engineering, Huzhou University, Huzhou 313000, Zhejiang, China*;
2. *Liaoning Provincial Institute of Agricultural Mechanization, Shenyang 110161, China*;
3. *Key Laboratory of Remanufacture and Innovation of Agricultural Machinery and Equipment, Liaoning Province, China*;
4. *Zhejiang Kingland Pipeline and Technologies Co., Ltd, Huzhou 313000, Zhejiang, China*;
5. *Huzhou College, Huzhou 313000, Zhejiang, China*)

Abstract: Multi-subsoiler collaboration plays a significant role in improving the efficiency of subsoiling. High tillage resistance during subsoiling seriously affects consumption, and the excessive soil disturbance may result in an increase in the amount of water that evaporates from the soil, which is unfavorable for water conservation. However, the space arrangement and types of subsoiler are key parameters for design of a set of subsoilers and have a major effect on tillage resistance and soil disturbance, which is a critical performance indicator of subsoiling. In this paper, a set of subsoiler models were developed using DEM. A field experiment was conducted in the sowing season in an experimental field of 1 hm^2 with black soil of Juliangtun Village, Liaoning Province. In both the simulation and experiment, six types of subsoilers (TC-SM, TC-SC, TA-SM, TA-SC, TDW-SM, and TDW-SC) were investigated at three different spacing arrangements (500, 600, and 700 mm), a constant vertical distance between the front and back subsoilers (500 mm), a constant working speed (3 km/h), and a constant working depth (400 mm). The mechanism of resistance was analyzed. The results showed that the tillage resistances of the six types of subsoilers were in the descending order of $F_{TDW\text{-}SC}$>$F_{TA\text{-}SC}$>$F_{TC\text{-}SC}$>$F_{TDW\text{-}SM}$>$F_{TA\text{-}SM}$>$F_{TC\text{-}SM}$. The field test showed that TC-SM with 600 mm spacing produced stable fluctuations with less tillage resistance. The variance analysis and regression equation testing of the experimental results were analyzed to enhance their scientific rigor. The analysis showed that the significances of each factor on the results were in the descending order of shank, space, and tine. The optimal configuration may be with spacing of 600 mm, tine of TC, and shank of SM, which is consistent with the field test and theoretical analysis. Tillage resistance of the DEM simulation was less than that of the field experiment, with an error of less than 10%, due to ignoring the effect of crop roots, straw residue, stones, or blunt tine and shank, which confirms the authenticity of simulation. The effect of spacing on soil disturbance behavior indicates that a mixed soil structure with moderate soil disturbance and soil porosity ratio and a spacing of 600 mm would be a good choice. This study provides an important foundation in selecting spacing for subsoiling to achieve an optimal soil tillage condition.

Keywords: subsoiler, space arrangement, mechanism analysis, tillage resistance, soil disturbance
DOI: 10.25165/j.ijabe.20251801.8996

Citation: Wang Y M, Lu C J, Fan J J, Zhang X, Chen K, Chen J, et al. Evaluating the effects of subsoiler type and spacing on tillage resistance and soil conservation with DEM simulation and field experiment. Int J Agric & Biol Eng, 2025; 18(1): 115–123.

1 Introduction

Liaoning Province is the largest grain crop producer in China, accounting for about 61% of the land area dedicated to cultivation of grain crops in the country. Due to the problems of low temperature and poor moisture content during spring sowing in Liaoning Province, agricultural production is seriously affected. In addition, traditional tillage methods, such as long-term rotary tillage and plow tillage, cause serious degradation of soil structure, and deepen and thicken the bottom layer of the plowed soil, which will affect the development of crop roots and the absorption of water and nutrients in the soil, seriously impeding sustainable crop production[1,2]. Conservation tillage has been the main planting mode to solve the above problems[3].

Subsoiling technology, as one of four technologies of conservation tillage, has received more and more attention. Mechanical subsoiling is the most widely used and rapid solution to improve soil compaction[4]. Subsoiling can effectively improve the soil's physical characteristics and enhance the basic soil fertility of cultivated land, which improve the crop yield and maintain the farmland's ability for high yields. At present, there are four main problems in the subsoiling process at home and abroad. Firstly, large resistance leads to easy deformation of the subsoiler[5]. Secondly, the subsoiler space dislocation arrangement mode is unreasonable, resulting in an overall energy consumption increase[6]. Thirdly, the depth of subsoiling is generally less than 30 cm, which

Received date: 2024-04-16 **Accepted date:** 2024-12-02
Biographies: Yueming Wang, PhD, Lecturer, research interest: agricultural mechanization engineering, smart materials, Email: 468119083@qq.com; **Chenjie Lu**, Undergraduate, research interest: agricultural mechanization engineering, Email: 17858360426@163.com; **Jiajun Fan**, MS candidate, research interest: mechanization engineering, Email: 1287978343@qq.com; **Xu Zhang**, MS, Senior Engineer, research interest: agronomy, Email: lnami@126.com; **Kai Chen**, Senior Engineer, research interest: materials science, Email: 504348900@qq.com.

***Corresponding author: Jing Chen**, MS, Senior Agronomist, research interest: agricultural mechanization and automation. Liaoning Provincial Institute of Agricultural Mechanization, Shenyang 110161, China. Tel: +86-15942317888, Email: 169333333@qq.com; **Xiaoguang Li**, PhD, Lecturer, research interest: control engineering. Huzhou College, Huzhou 313000, Zhejiang, China. Tel: +86-18540380855, Email: lixiaoguang@zjhzu.edu.cn.

cannot meet the different subsoiling requirements under different soil conditions[7]. Fourth, excessive soil disturbance causes the soil to turn over and reduces moisture retention[2].

However, despite the widespread use of this type of deep tillage, its effectiveness and sustainability are disputed. Previous studies show a great variety of outcomes depending on soil texture, soil moisture content, weather conditions, and subsequent field operations, but the effects of the wide variety in available subsoilers have remained understudied. The subsoiler is a direct contact soil component in the subsoiling process. Its structural characteristics determine the tillage resistance. At present, the research mainly focuses on the application of bionic principles to improve resistance reduction performance. For example, the key components of subsoiling are optimized based on the biological surface microstructures of the brown bear, pangolin, and dung beetle. The electron permeability of the soil parts is designed based on the earthworm's characteristics. Some scholars also use the method of vibration subsoiling to achieve the purpose of reducing resistance, but only under specific conditions[8]. At present, it mainly targets a single arrangement of a subsoiler type to examine its subsoiling performance under the same soil conditions. Actually, in order to increase the subsoiling efficiency, more subsoilers cooperation is needed. However, the subsoilers layout is based on experience, without correlation analysis, which will cause a poor tillage effect, tillage resistance, and other problems. At the same time, subsoiling speed, subsoiler structure, and space dislocation arrangement between subsoilers have a significant impact on tillage resistance, wear performance, and soil disturbance effect. There are very few systematic studies on soil conditions, operating parameters, subsoiler type, and spatial arrangement[9]. Therefore, it is urgent to select a different subsoiler structure with multi-tip interaction and layout mode to reduce the tillage resistance and soil disturbance.

Traditional subsoilers typically feature a straightforward design with one or more shanks arranged in a straight line, intended to penetrate the soil and break up compacted layers beneath the plow depth. However, these subsoilers have limited soil disturbance, primarily affecting the soil aligned with the subsoilers, and tend to create new compacted layers below the working depth, consume high energy, and lack adaptability to varying soil conditions[10]. These limitations lead to low operational efficiency, poor soil improvement, and high energy consumption. This study's innovative subsoiler design addresses these drawbacks with an optimized wing design that increases soil disturbance and reduces new compaction, precision agriculture integration for real-time adjustments, and an adjustable depth control system for consistent and efficient subsoiling, improving soil health and crop yields.

When operating, especially in hard soil, a subsoiler is subjected to immense stress and torque. If the structural design is unreasonable and lacks sufficient rigidity, prolonged use may lead to deformation. This deformation can result in uneven subsoiling depth, affecting the quality of operation. Additionally, long-term stress concentration accelerates metal fatigue, which may ultimately cause fractures[11]. The tines are the components in direct contact with the soil, and their shape, angle, and material directly affect the subsoiling performance. Poorly designed tines can easily get damaged in high-resistance soil, leading to frequent replacements and increased maintenance costs. If the tine angle is too large or too small, it will affect the soil penetration and loosening effects.

Subsoiling is a complicated process. When a subsoiler passes through the soil, soil loosening, movement, and mixing will cause soil disturbance. Subsoiling tillage aims to loosen the compacted soil layer to improve water content and air permeability, without damaging the surface vegetation and disturbing the soil layer. That is, it increases the porosity of the bottom layer without flipping the other soil layers. Conventional experimental methods are time-consuming without fully and precisely describing the disturbance regime of soil layers[12]. DEM (discrete element method) is an analytical method to deal with discontinuous media problems which is being widely used in research on dynamic simulation of granular objects, such as soil analysis applications. It can simulate the viscous behavior between tillage parts and soil to predict soil disturbance characteristics. Therefore, DEM numerical simulation methods are used to simulate a subsoiling process to describe the soil disturbance.

In this study, the research was carried out to investigate the effects of different space arrangements and types on the characteristics of tillage resistance on the field experiment. The mechanism of resistance with different tines and shanks is also analyzed to illuminate the influence of different subsoilers on tillage resistance. Then, the effect of spacing on soil disturbance behavior and tillage resistance using DEM is discussed. Based on the results of the above, the optimal space arrangement and type are determined. This provides an important foundation for the study of the resistance reduction mechanism and the resistance reduction and loss reduction structure of agricultural machinery soil contact components.

2 Materials and methods

2.1 Experimental materials and modeling construction

Based on JB/T 9788-2014, subsoiler tines can be divided into double wing tine (TDW), arrow tine (TA), and chisel tine (TC) types. Shanks include light shank (SL), medium shank (SM), and column shank (SC). Due to the bending and fracture of SL during the test, only SM and SC are used in this paper. Both of the subsoilers are made of 65 Mn steel.

Six kinds of models are constructed: TC-SM, TC-SC, TA-SM, TA-SC, TDW-SM, and TDW-SC (Figure 1). A tractor is used as traction gear for subsoiling work. Subsoilers are fixed to the rack with a certain front and rear size. Subsoilers are arranged in triangles with apace dislocation sizes (Figure 1). The vertical distance between the front and back subsoiler is 500 mm. The distances between the back subsoilers are 500, 600, and 700 mm, respectively.

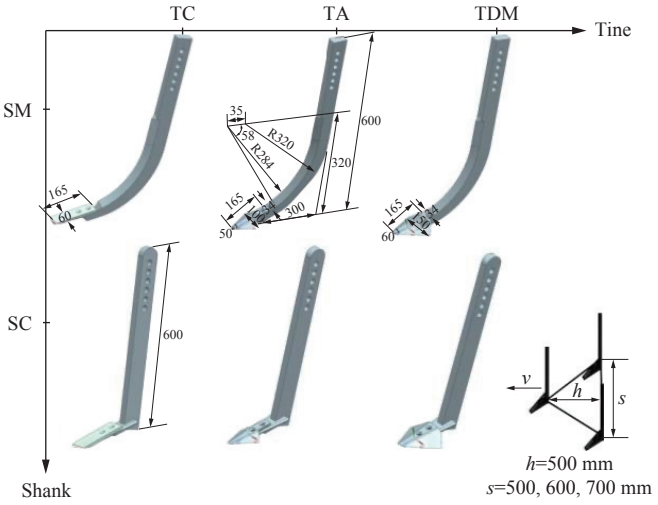

Figure 1 Different tine-shank model and multi-subsoiler cooperation mode

2.2 Experimental process

A field experiment was conducted in the sowing season in an experimental field of 1 hm^2 with black soil of Juliangtun Village, Liaoning Province (Figure 2). The subsoiler, sensors, and data acquisition device are connected to the tractor correctly, and equipment functionality is first checked to ensure normal operation. Considering the instability of soil disturbance during start-up and stopping phases, each test plot includes three distinct sections, a 10-m adjustment region on each side, and a 50-m stabilized center section as the data acquisition region. Improving the operation speed can shorten the loading time on the soil and reduce the soil compaction[12]. However, an excessive speed will increase the soil disturbance. Therefore, the optimal subsoiling parameters are set at a speed of 3 km/h and subsoiling depth of 400 mm.

Figure 2 Field experiment

BK-1 type sensor is selected with power supply of 24 VDC, measuring range of 0-30 kN, and output of 4-20 mA. The pull-up rod sensor and the two-pin suspension sensor are connected to the tractor power take-off shaft by means of a three-point suspension. Data collection is set at a frequency of 5 Hz; that is, data points are collected every 0.2 s.

In general, the tractor initially enters a 10-m debugging section, lowering the subsoiler to the target tillage depth of 400 mm via the hydraulic system and maintaining this depth. The tractor is then set to operate at specified subsoiling speeds of 2 km/h and 3.6 km/h. Upon entering the 50-m test section, data is collected and stored. This field experiment is a comprehensive test, with each group of trials repeated three times, and the average of the three trials is taken as the tillage resistance value for this subsoiler.

2.3 Soil conditions

The soil used in this experiment is black soil from Juliangtun Village, Liaoning Province. It exhibits a loam to clay loam texture, characterized by a well-aggregated granular structure that supports both water retention and aeration. Its soil particle composition typically includes 30%-40% clay, providing the soil with high plasticity and moisture-holding capacity. The silt content ranges from 20%-30%, contributing to the soil's softness and drainage properties. Sand particles, at less than 20%, are relatively low, enhancing the soil's nutrient retention and making it highly fertile for agricultural use. These soil parameters affect its moisture content and hardness, thereby influencing the tillage resistance and soil disturbance during subsoiler operations.

In this experiment, the soil cone index (CI) of the 0-50 mm, 50-150 mm, 150-250 mm, and 250-350 mm layers was measured by cone penetrometer of SC 900 (RGB Spectrum Equipment, USP) with a 1/2″ diameter cone tip, with 10 test points for each layer. The average value was taken as the soil CI of that layer, as shown in Figure 3.

Soil moisture content affected the tillage resistance and soil disturbance. Corresponding to soil compaction, the soil moisture contents were also measured in the 0-50 mm, 50-150 mm, 150-250 mm, and 250-350 mm layers (10 test points for each layer) by the weighing method under an outdoor temperature of 18°C. The soil moisture content was calculated as follows:

$$\eta = \frac{M_1 - M_2}{M_1} \times 100\% \tag{1}$$

where, η is the soil moisture content, %; M_1 is the wet weight of soil sample, g; and M_2 is the dry weight of soil sample, g. The average is taken as the value of the soil moisture content of that layer (Figure 3). The figure shows that the root growth part lacks water with the reduced soil moisture content at 250 mm. So, subsoiling is necessary for soil moisture conservation cultivation.

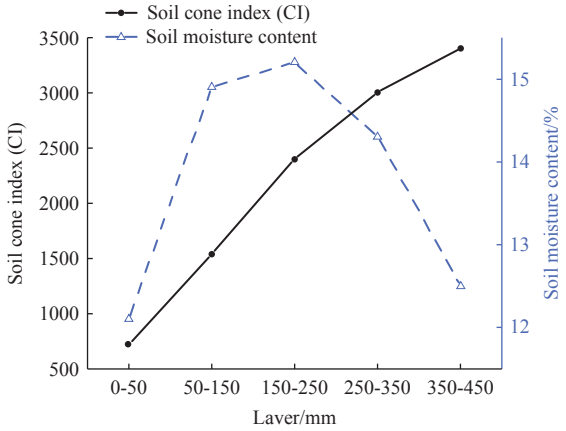

Figure 3 Soil compaction and moisture content of different tillage layers in the experimental area

2.4 DEM modeling construction

DEM is an analytical approach for handling problems involving discontinuous media, making it suitable for dynamic simulations of granular materials, such as soil analysis applications. The classic discrete element model is used to calculate the interaction forces between soil particles. The force model consists of normal force (F_n), cohesive force (F_c), shear force (F_s), friction force (F_f), and gravitational force (F_g), as shown in Figure 4. The bonding force between two particles is the result of the combined action of the micro-cohesive force and micro-friction force. The micro-cohesive force acts in the normal direction, causing the particles to connect and overlap to some extent; when particles slide, a micro-friction force is generated in the tangential direction[13]. In the following equations, the units of parameters are international standard units, such as force of N, torque of N·m, and mass of kg. The remaining parameters are dimensionless.

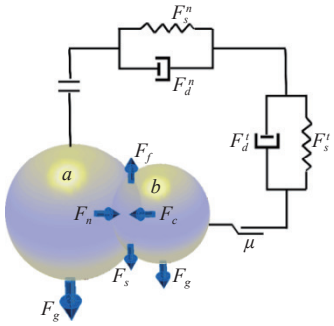

Figure 4 Discrete element model and contact force diagram

In DEM simulation process, based on a given time increment, the relative displacement and relative velocity between two particles, *a* and *b*, are calculated in terms of their normal and tangential components. Due to the creep properties of viscoelastic materials, the *Kelvin* model is used to describe the bonding forces between particles. This is represented by normal elastic force (F_s^n), normal viscous force (F_d^n), tangential elastic force (F_s^t), and tangential viscous force (F_d^t) to express the mechanical properties between the particles[14]. The elastic force can be expressed as a function of stiffness and relative displacement, while the viscous (damping) force is described as a function of the damping coefficient and relative velocity.

The expressions for the normal force F^n and tangential force F^t are as follows:

$$F^n = F_s^n + F_d^n \tag{2}$$

$$F^t = F_s^t + F_d^t \tag{3}$$

According to Coulomb's law of friction, the tangential force should be less than the maximum frictional force; therefore,

$$F^t = \begin{cases} F^t (F^t < \mu \cdot F^n) \\ \mu \cdot F_s^n (F^t \geq \mu \cdot F^n) \end{cases} \tag{4}$$

where, μ is the friction coefficient.

Resultant of forces F^{res} can be expressed as follows:

$$F^{res} = \vec{F}^n + \vec{F}^t + \vec{F}_g \tag{5}$$

The tangential component of the force generates an instantaneous moment M^t, which can be expressed through the tangential force and the distance (l) between the particle and the contact point.

$$M^t = F^t \cdot l \tag{6}$$

In a granular system, the rotation of particles generates rolling resistance, which consumes energy while providing support to the system, ensuring the stability of the granular assembly. The moment generated by rolling friction M^r is as follows.

$$M^r = \mu^r \cdot F_s^n \cdot l \cdot \omega \tag{7}$$

where, μ^r is the coefficient of rolling friction; ω is the contact point angle velocity unit vector.

Resultant of moment M^{res} is shown as follows:

$$M^{res} = \vec{M}^t + \vec{M}^r \tag{8}$$

According to Newton's Second Law, the particle's acceleration can be calculated. The translation acceleration (a^{tra}) and rotational acceleration (a^r) of the particle are solved as follows:

$$a^{tra} = \frac{F^{res}}{m} \tag{9}$$

$$a^r = \frac{M^{res}}{M_0} \tag{10}$$

where, m is particle mass; M_0 is particle initial moment.

By using Equations (9) and (10), the particle velocity can be obtained, and by integrating over the time interval, the new position of the particle can be calculated.

Assuming that the deformation at the contact point is nonlinear elastic deformation, it means that the loading and unloading cycles follow the same path. The Hertz-Mindlin contact model is chosen with the cohesive force between the two particles of zero.

In the Hertz-Mindlin contact model, the normal elastic force F_s^n between particles is defined as follows:

$$F_s^n = -K^n \cdot (l^n)^{3/2} \tag{11}$$

where, l^n is normal component of the relative displacement between the particles; K^n is normal stiffness, $K^n = 2 \cdot E' \cdot \sqrt{r' \cdot l^n}$; E' is equivalent Young's modulus, $\frac{1}{E'} = \frac{(1-\nu_a^2)}{E_a} + \frac{(1-\nu_b^2)}{E_b}$; E_a is Young's modulus of particle *a*; E_b is Young's modulus of particle *b*; ν_a is Poisson's ratio of particle *a*; ν_b is Poisson's ratio of particle *b*; r' is equivalent radius, $\frac{1}{r'} = \frac{1}{r_a} + \frac{1}{r_b}$; r_a is radius of particle *a*; r_b is radius of particle *b*.

The tangential elastic force F_s^t can be expressed as follows:

$$F_s^t = -K^t \cdot l^t \tag{12}$$

where, l^t is tangential component of relative displacement between particles; K^t is tangential stiffness, $K^t = 8 \cdot I' \cdot \sqrt{r' \cdot l^n}$; I' is equivalent elastic modulus, $\frac{1}{I'} = \frac{2-\nu_a}{I_a} + \frac{2-\nu_b}{I_b}$; I_a is equivalent elastic modulus of particle *a*; I_b is equivalent elastic modulus of particle *b*.

The normal viscous force F_d^n and the tangential viscous force F_d^t can be expressed as follows:

$$F_d^n = -2 \cdot \zeta \cdot l^n \cdot \sqrt{\frac{5}{6} K^n \cdot m'} \tag{13}$$

$$F_d^t = -2 \cdot \zeta \cdot l^t \cdot \sqrt{\frac{5}{6} K^n \cdot m'} \tag{14}$$

where, m' is equivalent mass, $\frac{1}{m'} = \frac{1}{m_a} + \frac{1}{m_b}$; m_a is mass of particle *a*; m_b is mass of particle *b*; ζ is damping ratio, $\zeta = \frac{\ln e}{\sqrt{\ln^2 e + \pi^2}}$; e is the particle recovery coefficient.

In the simulation, the material parameters for the subsoilers are set according to the material parameters of 45# steel. In Northeast China, the primary cultivated soil is viscous and prone to clumping, commonly adhering to the surface of soil-contacting components. According to relevant literature[15,16], the parameter settings for the discrete element simulation are listed in Table 1.

Table 1 Basic parameters of the DEM

Parameters	Value
Density of subsoiler (65 Mn steel)/kg·m^{-3}	7830
Poisson's ratio of 65 Mn steel	0.35
Shear modulus of 65 Mn steel/MPa	7.27×10^4
Density of soil/kg·m^{-3}	1800
Poisson's ratio of soil	0.40
Bond stiffness of layers/N·m^{-3}	5×10^7
Critical stresses of the bond of layers/Pa	4×10^4
Shear modulus of soil/MPa	70
Radius of the bond of soil/mm	8.36
Coefficient of rolling friction in soil	0.56
Coefficient of rolling friction between soil and 65 Mn steel	0.38
Coefficient of restitution between materials	0.6
Coefficient of static friction between soils	0.4
Coefficient of static friction between soil and subsoiler	0.5

Soil particles with radius of 4-6 mm are randomly generated in a 2000 mm×1000 mm×800 mm soil tank (Figure 5). To better analyze the soil disturbance characteristics, the soil is set to five layers, each with a height of 86 mm. The 3D subsoiler models are introduced into DEM until the particle settlement stabilizes. The simulation parameters are the same as those of the field experiments.

2.5 Mechanism analysis of resistance with different tine and shank

According to the Mohr-Coulomb strength theory, when the Mohr circle reaches the Coulomb envelope, the critical bonding lines of the normal stress and shear stress that cause soil failure can be obtained. The soil failure line equation is as follows. Its intercept is equal to the cohesion of the soil, and the slope is equal to the friction within the soil.

$$\tau_f = c + \sigma \tan\theta \tag{15}$$

where, τ_f is soil shear strength, MPa; c is cohesive strength of soil, MPa; σ is normal compressive stress on the shear failure surface, MPa; θ is angle of internal friction in soil, (°).

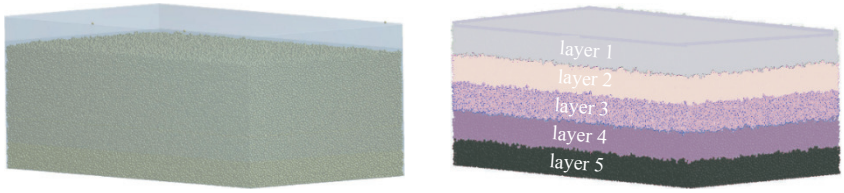

a. Soil bin created by DEM b. Soil layers

Figure 5 Soil tank model

In the process of soil separation, the traction resistance required by the subsoiler is composed of the force generated by the subsoiling speed and the tillage resistance required by the shank and the tine. The resistance generated by the working speed of the subsoiler can be calculated by the wingspan of the subsoiler, the working depth, the friction angle in the soil, the soil density, and the forward speed[17]. The resistance generated by the shank and tine during subsoiling consists of the forces generated when the soil is cut and rubbed against it. The force generated by cutting the soil is related to the wingspan of the subsoiler, the working depth, the angle of friction in the soil, and the density of the soil.

When the tine of the subsoiler cuts the soil forward, the clod above the tine first experiences shear failure. Force analysis of TC, TA, and TDW surface and the soil on the tine is shown in Figure 6. The tine (TC, TA, and TDW) is subjected to traction (F_{tine}), soil pressure (N_1), friction between the subsoiler and the soil ($\mu_{\text{tine-soil}}N_1$), subsoiler penetrating angle (α), and cutting resistance (kb).

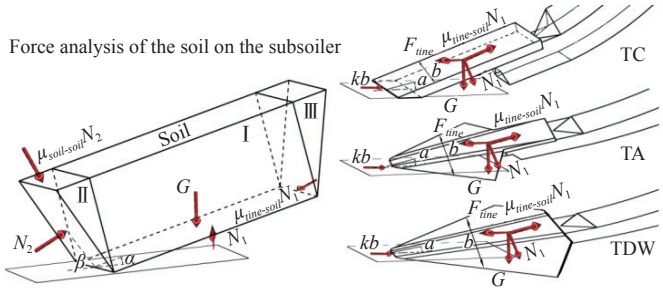

Figure 6 Force analysis of TC, TA, and TDW surface and the soil on the subsoiler

According to the law of mechanical equilibrium, the force balance equation for the horizontal direction of the tine is as follows:

$$F_{tine} = N_1 \sin\alpha + \mu_{tine\text{-}soil} N_1 \cos\alpha + kb \tag{16}$$

The equation of soil equilibrium mechanics at the top of the tine can be expressed as follows:

$$G - N_1(\cos\alpha - \mu_{tine\text{-}soil}\sin\alpha) - N_2(\cos\beta - \mu_{soil\text{-}soil}\sin\beta) + (cS_1 + B)\sin\beta = 0 \tag{17}$$

$$N_1(\sin\alpha + \mu_{tine\text{-}soil}\cos\alpha) - N_2(\sin\alpha + \mu_{soil\text{-}soil}\cos\beta) - (cS_1 + B)\cos\beta = 0 \tag{18}$$

where, G is soil gravity on the subsoiler surface; N_2 is normal load on front failure surface of soil; S_1 is area of the front shear failure surface of soil; β is slope angle of the front failure surface of the soil; B is the acceleration force of the soil driven by the tine. According to Newton's second law, B is as follows:

$$B = Ma = M\frac{\mathrm{d}v_{soil}}{\mathrm{d}t} \tag{19}$$

where, a is soil acceleration, m/s²; v_{soil} is the velocity of the soil disturbed by the tine, m/s. It can be approximated as the speed of the subsoiler, that is, the speed of subsoiling operation. M is the soil quality disturbed by the tine. As shown in Figure 6, it is composed of Ⅰ, Ⅱ, and Ⅲ three parts, and the range of soil disturbance can be made as an isosceles trapezoidal with a vertex angle of (π/8+π/2).

It can be obtained from Equations (16)-(18):

$$F_{tine} = \frac{G}{K_1} + \frac{cS_1 + B}{K_1(\sin\beta + \mu_{soil-soil}\cos\beta)} + kb \tag{20}$$

where, $K_1 = \dfrac{\cos\alpha - \mu_{tine\text{-}soil}\sin\alpha}{\sin\alpha + \mu_{tine\text{-}soil}\cos\alpha} + \dfrac{\cos\beta - \mu_{soil-soil}\sin\beta}{\sin\beta + \mu_{soil-soil}\cos\beta}$.

The soil gravity G on the tine is as follows:

$$G = \int \rho_{soil} S_2 g \mathrm{d}h \tag{21}$$

where, S_2 is the area of soil acting on the tine.

So, F_{tine} is in proportion to S_2 and b. For TC, TA, and TDW, S_{2TDW}>S_{2TA}>S_{2TC}, b_{TDW}>b_{TA}>b_{TC}. So, $F_{tineTDW}$> F_{tineTA}> F_{tineTC}.

Force analysis of the soil unit on the shank is shown in Figure 7.

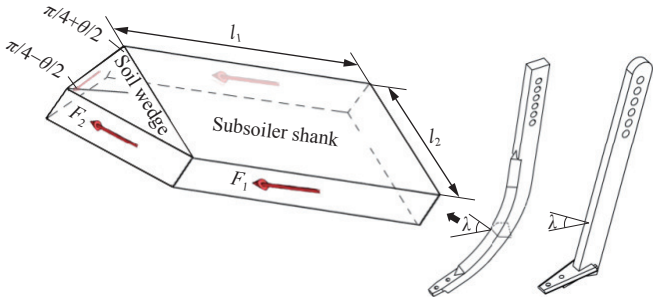

Figure 7 Force analysis of the soil on the shank

According to the passive soil failure theory, the angle between the side of the soil wedge and the forward direction is π/4+θ/2.

$$F_{shank} = 2\left(\int \mathrm{d}F_1 + \int \mathrm{d}F_2 \cos\left(\frac{\pi}{4} - \frac{\theta}{2}\right)\right)\cos\lambda \tag{22}$$

where, λ is the normal angle between the soil unit and shank.

The force generated by the friction of the shank against the soil unit F_{shank} consists of two parts: the friction between shank and soil unit F_1, and the friction between soil unit and soil unit F_2. So, F_{shank} can be expressed as follows:

$$F_{shank} = 2\left(\int \mu_{tine\text{-}soil} \mathrm{d}N_1 + \int \mu_{soil-soil} \mathrm{d}N_2 \cos\left(\frac{\pi}{4} - \frac{\theta}{2}\right)\right)\cos\lambda = 2\left(\int \mu_{tine\text{-}soil}\sigma_h \mathrm{d}A_1 + \int \mu_{soil-soil}\sigma_h \mathrm{d}A_2 \cos\left(\frac{\pi}{4} - \frac{\theta}{2}\right)\right)\cos\lambda \quad (23)$$

where, N_1 is the normal force acting on the soil unit on the side of the shank; N_2 is the normal force acting on the soil unit in front of the shank; $\mathrm{d}A_1$ is soil unit area on the side of the shank, $\mathrm{d}A_1 = 2l_1\cos\lambda\mathrm{d}z$; $\mathrm{d}A_2$ is soil unit area on the side of the shank, $\mathrm{d}A_2 = \dfrac{l_2}{2\cos\left(\frac{\pi}{4} + \frac{\theta}{2}\right)}\cos\lambda\mathrm{d}z$; σ_h is horizontal normal stress generated by soil unit.

$$F_{shank} = 2\left(\int 2\mu_{tine\text{-}soil}\sigma_h l_1 \mathrm{d}z + \int \mu_{soil-soil}\sigma_h l_2 \frac{\cos\left(\frac{\pi}{4} - \frac{\theta}{2}\right)}{2\cos\left(\frac{\pi}{4} + \frac{\theta}{2}\right)}\mathrm{d}z\right)\cos^2\lambda \quad (24)$$

So, F_{shank} is in proportion to $\cos^2\lambda$. For SM and SC, $\lambda_{SC}<\lambda_{SM}$. So, $F_{shankSC} > F_{shankSM}$.

The resistance F_t generated by soil-soil friction is the sum of F_{shank} and F_{tine}, that is, $F_t = F_{shank} + F_{tine}$. That is, $F_{TDW\text{-}SC}>F_{TA\text{-}SC}>F_{TC\text{-}SC}>F_{TDW\text{-}SM}>F_{TA\text{-}SM}>F_{TC\text{-}SM}$.

3 Results and discussion

3.1 Effect of subsoiler type and spacing on tillage resistance with field test

To investigate the actual tillage performance, the field experiments of TC-SM, TC-SC, TA-SM, TA-SC, TDW-SM, and TDW-SC were carried out at a speed of 3 km/h under different spacing arrangements in the sowing season of 2022 in an experimental field of 1 hm², with black soil of Juliangtun Village, Liaoning Province (Figure 2). Tillage resistance fluctuates around a fixed value, as shown in Figure 8. In the process of interaction between subsoiler and soil, the soil is regarded as a combination of countless soil block units. The interaction first causes the soil block to produce elastic deformation. Then, when the limit state is reached, plastic deformation occurs and micro-cracks are generated[18]. As the subsoiler continues to advance, the crack expands until it breaks the clod. This process is repeated for the next clod cell. The fluctuation of resistance reflects the continuous periodic failure of the soil block during subsoiling[19]. The force-displacement curves show that TC-SM produces stable fluctuations and less tillage resistance.

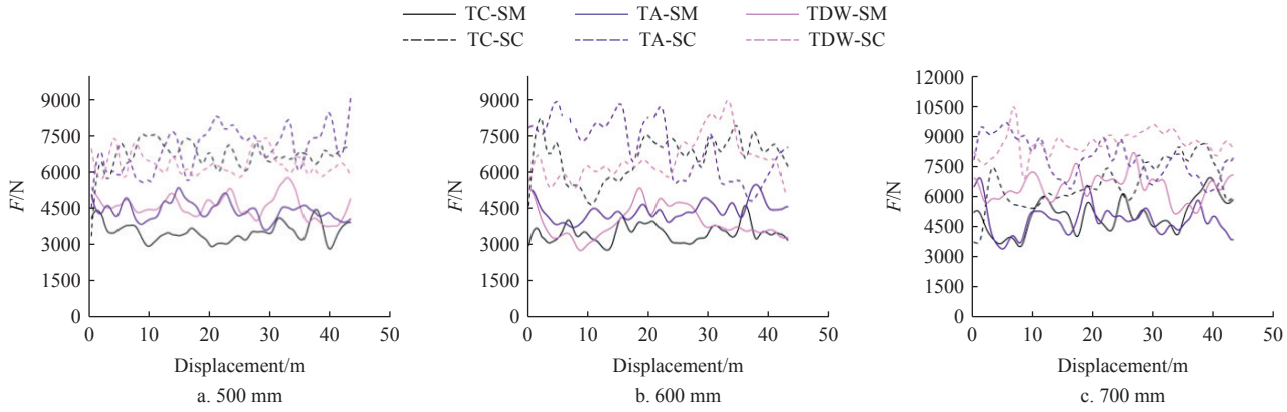

Figure 8 Tillage resistance of TC-SM, TC-SC, TA-SM, TA-SC, TDW-SM, and TDW-SC under different spacing arrangements

The average tillage resistance of TC-SM, TC-SC, TA-SM, TA-SC, TDW-SM, and TDW-SC with different spacings are shown in Figure 9. The shank and tine of the subsoiler squeeze the soil at the same time and produce cutting during subsoiling. The cut soil continues to move backwards. The moving soil is subjected to the intense extrusion of the blade surface of the subsoiler and shear failure occurs[9]. The friction between the tine, the blade of the shank, and the surface of the blade with the soil, as well as the friction within the soil particles, produces a soil driving layer. Due to its internal velocity gradient, the inside soil driven by the moving soil layer is squeezed and rubs against the soil layer, then breaks. The subsoiler has the least resistance at 600 mm spacing compared with that of 500 mm and 700 mm. This is consistent with the theoretical analysis: $F_{TDW\text{-}SC}>F_{TA\text{-}SC}>F_{TC\text{-}SC}>F_{TDW\text{-}SM}>F_{TA\text{-}SM}>F_{TC\text{-}SM}$.

There is no interaction between the variables. A multi-factor analysis of variance is conducted for each variable. Firstly, the experimental variables in algebraic terms are expressed, such as S(1)=500, S(2)=600, S(3)=700, T(1)=TA, T(2)=TDW, T(3)=TC, SH(1)=SM, and SH(2)=SC, and the tillage resistance results are standardized. The standardization process is as follows: $Y_{standard} = (Y_i - \overline{Y})/s^2$, where, Y_i is the tillage resistance of every sample; $\bar{Y}$ is the mean of tillage resistance; s^2 is sample variance. The results of the variance analysis are listed in Table 2.

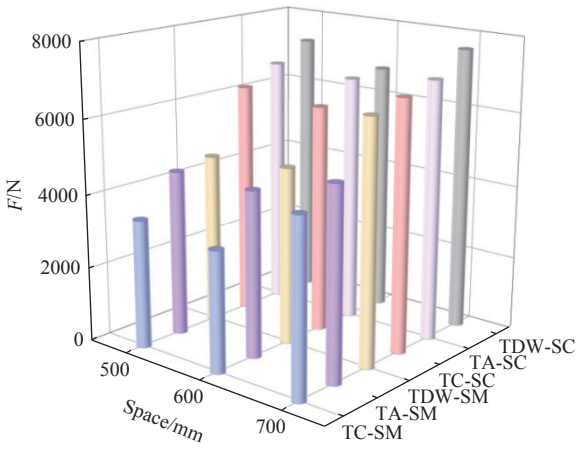

Figure 9 Average tillage resistance of TC-SM, TC-SC, TA-SM, TA-SC, TDW-SM, and TDW-SC with different spacings

Table 2 Results of the variance analysis

Parameters	F	p	R^2
Space	4.413	0.037	
Shank	61.862	<0.001	0.862
Tine	2.058	0.170	

From Table 2, it can be seen that the significance of each factor on the results is in the descending order of shank, space, and tine.

When establishing the regression equation, due to the influence of numerical relationships among the algebraic terms of each variable, dummy variables are created using the first level of each factor as the reference. This converts numerical relationships into binary relationships (presence or absence). Similarly, a regression equation is established using the standardized experimental results as the output. The parameter test of the regression equation is conducted, as listed in Table 3.

Table 3 Parameter test of the regression equation

Parameters	β	t	p
S(2)	–0.049	–0.395	0.700
S(3)	0.292	2.352	0.037
T(2)	–0.034	–0.271	0.791
T(3)	–0.233	–1.877	0.085
SH(2)	0.844	7.865	<0.001

In this experiment, resistance is the output, with lower resistance indicating better performance. Thus, a lower *Beta* value in the table is preferable. The table shows that the significance of factor S(2) relative to S(1) is 0.7, indicating that S(1) and S(2) have a similar impact on the experiment overall, with minimal difference in results between spacings of 500 and 600 mm. The significance of S(3) is 0.037, indicating a greater impact on the overall experiment, but its *Beta* value is positive, meaning it increases resistance, while S(2) has a negative β value, suggesting it may perform better than S(1). Similarly, T(3) and SH(1) are the optimal levels. Thus, the optimal configuration may be with spacing of 600 mm, tine of TC, and shank of SM, which is consistent with the field test and theoretical analysis.

3.2 Influence of TC-SM and TA-SM on tillage resistance with DEM simulation

Although DEM is used widely and its results are valuable in agriculture, the validation experiments are conducted considering credibility. From the field test, it is evident that TC-SM and TA-SM have less resistance. So, the influences of TC-SM and TA-SM on tillage resistance with DEM are compared with those of the field test to discuss the authenticity of the simulation. In this simulation, the forward speed of the subsoiler is set to 3 km/h, and the penetrating angle is set to 20°, consistent with the parameters of the actual field test. The soil penetration depth is also nearly identical to the real field test depth. These settings ensure a high level of consistency between the simulation results and actual field conditions, aiding in verifying the reliability of the simulation results and providing data support for further optimization of the subsoiler design. Taking TC-SM as an example, the interaction between the subsoilers and the soil proceeds through four main stages, as shown in Figure 10: a) the fore subsoiler just contacting the soil; b) the subsoilers fully immersing in the soil; c) the fore subsoiler just leaving the soil; and d) the rear subsoilers fully out of the soil. From stage (a), when the fore subsoiler starts to contact the soil, the tillage resistance increases suddenly because of the broken soil[10]. From stage (b) to (c), the subsoilers immerse in the soil completely, and enter the stable fluctuation stage. Generally, the average value of this stage is used as the tillage resistance. That is, the data from stage (b) to (c) is the valid data to calculate the tillage resistance. From stage (d), the rear subsoilers are fully out of the soil.

The tillage resistance of TC-SM and TA-SM in the steady state are shown in Figure 11. In general, a lower tillage resistance indicates a better performance because it corresponds to a lower power requirement.

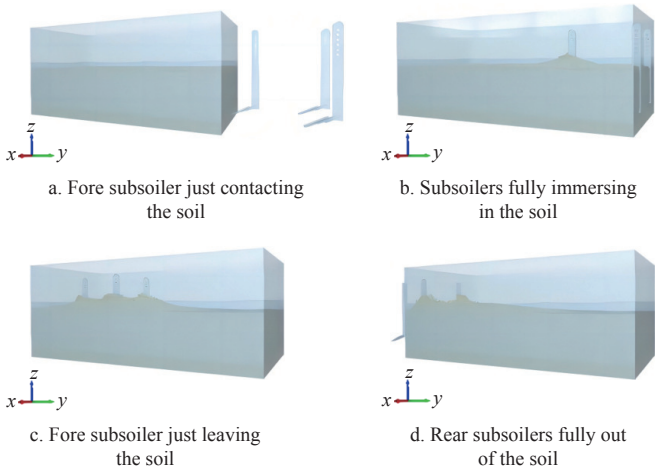

a. Fore subsoiler just contacting the soil

b. Subsoilers fully immersing in the soil

c. Fore subsoiler just leaving the soil

d. Rear subsoilers fully out of the soil

Figure 10 Four stages of the interaction between the subsoilers and the soil

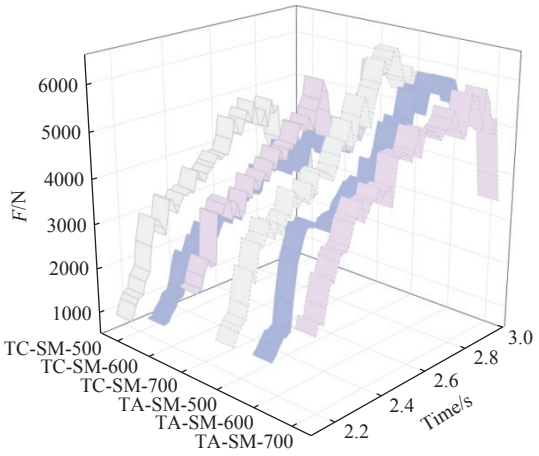

Figure 11 Tillage resistance of TC-SM and TA-SM with DEM simulation

The experimental and simulated tillage resistance values of TC-SM and TA-SM are presented in Table 4. After calibration, the DEM-predicted tillage resistance values are consistently within a 10% error range compared to the field test results, confirming the reliability of the simulations. According to Equation (16), kb, which represents pure cutting resistance, cannot be ignored when it is subjected to the presence of crop roots and straw residue in the field experiment twining around the subsoilers or the stones, causing large resistance and resulting in the blunting of the edge[20]. In simulation, the crop roots, straw residue, stones, or blunt subsoiler tines and shanks are not considered. Therefore, the tillage resistance in the simulation in DEM is smaller than that in the field, which is relatively reasonable and credible.

Table 4 Experimental and simulated tillage resistance of TC-SM and TA-SM

	F_{field}/N	$F_{simulation}$/N	Error
TC-SM-500	3478	3291	5.38%
TC-SM-600	3234	3072	5.01%
TC-SM-700	4699	4331	7.83%
TA-SM-500	4490	4238	5.61%
TA-SM-600	4481	4137	7.68%
TA-SM-700	5157	4675	9.35%

The use of discrete element method (DEM) simulations allows for a precise prediction of soil-tool interactions, which is a major step forward compared to traditional subsoiling models. This simulation approach helps minimize error margins, with the study achieving less than 10% deviation from field tests. This high level of accuracy enables better prediction and optimization of subsoiler performance.

3.3 Effect of spacing on soil disturbance behavior

When the subsoiler passes through the soil, the soil loosening, movement, and mixing are called soil disturbances. Subsoiling aims to loosen the compacted soil layer to improve water content and air permeability without flipping the soil layer. In general, the porosity of the soil layer and soil disturbance coefficient after subsoiling is used as an indicator of subsoiling performance. The shear and compressive forces exerted on the soil by the parts touching the soil are the main factors causing soil disturbance and movement. The disturbance characteristics and dynamic behavior of soil can be changed by changing the structure of soil-touching parts. According to the mechanism analysis of resistance with different tine and shank, during the process of subsoiling, the force that the subsoiler exerts on the soil, the type of subsoiler, and the contact area between soil and subsoiler are the main factors to explain the effect of spacings on soil disturbance behavior.

The soil disturbance is discussed by using the surface area of the cutting soil and the flipping soil. The subsoiling condition is demarcated by the natural contour of the soil after subsoiling and the internal soil disturbance contour. The schematic diagram is shown in Figure 12 to estimate the area between the contours by image representation. Curve fitting is carried out in CAD software to calculate the area size. The soil porosity ratio Y and soil disturbance coefficient X are as follows:

$$Y = \frac{D_2}{D_1} \times 100\% \tag{25}$$

$$X = \frac{D_3}{D_1} \times 100\% \tag{26}$$

where, D_1 is the cross-sectional area from the surface to the theoretical subsoiling; D_2 is the elevated soil area; D_3 is the disturbed soil area.

Soil disturbance profiles by the two rear TC-SM with different spacings of 500, 600, and 700 mm are shown in Figure 12.

By calculating the area ratio, the soil porosity ratio Y and soil disturbance coefficient X with different spacings of 500, 600, and 700 mm are shown in Figure 13. The soil disturbance coefficient is the greatest with a spacing of 500 mm, followed by a spacing of 700 and then 600 mm. There is not much difference between the soil porosity ratio with a spacing of 600 and 700 mm. This shows that the balanced soil disturbance between adjacent subsoilers can reduce the tillage resistance to a certain extent because of the lower soil gravity G on each tine according to Equation (21). The excessive soil disturbance may result in an increase in the amount of water that evaporates from the soil, which is unfavorable for water conservation and also consumes more energy for subsoiling. From the view of tillage performance and resistance, a mixed soil structure with moderate soil disturbance and soil porosity ratio, less force, and with a spacing of 600 mm would be a good choice. In summary, the spacing of subsoilers alters the soil disturbance characteristics and tillage resistance, which is very important in selecting spacing for subsoiling to achieve an optimal soil tillage condition.

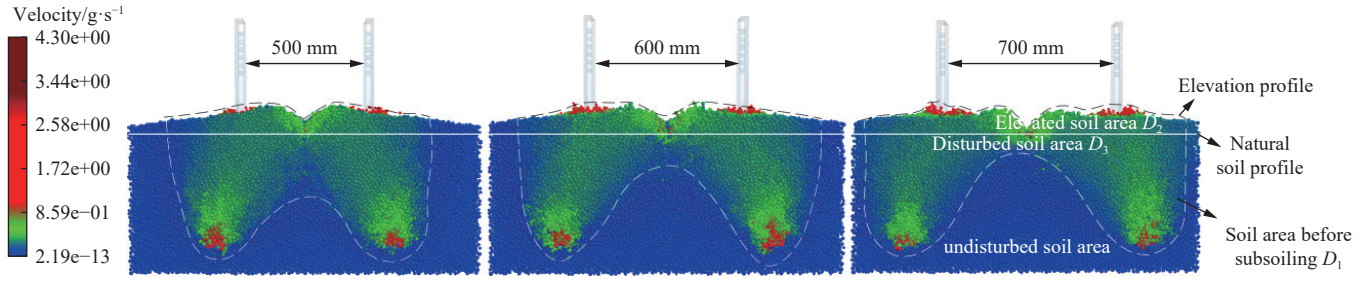

Figure 12 Simulated soil disturbance profiles by the two rear TC-SM with different tine spacings

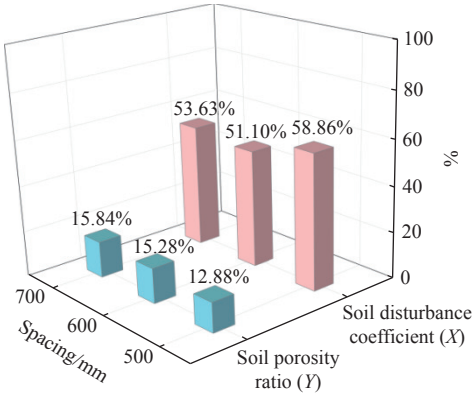

Figure 13 Soil porosity ratio (Y) and soil disturbance coefficient (X) with different spacings of 500, 600, and 700 mm

Simulated soil disturbance profiles by the fore and rear TC-SM with spacing of 600 mm are shown in Figure 13. It clearly indicates that the soil disturbance of the fore subsoiler is greater than that of

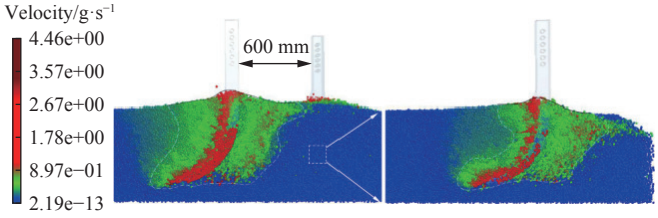

Figure 14 Simulated soil disturbance profiles by the fore and rear TC-SM with spacing of 600 mm

the rear. This is due to the soil disturbed by the fore subsoiler resulting in the increase of the porosity of the soil behind it, which reduces the tillage resistance of the rear subsoiler. At the same time, stress concentration is one of the important factors that cause the wear and deformation of subsoilers.

According to Figure 14, the stress concentration point of the subsoiler is mainly located at the lower end of the soil cutting edge, the junction of the handle and the tip, and the screw hole position of the connecting bolt with the tip. This is mainly due to the high shear force of the soil in the subsoiling process. Therefore, in the manufacturing process of the subsoiler, increasing the material strength of the cutting edge of the handle, the junction of the handle, and the bolt mounting hole is conducive to resisting stress concentration and improving the service life.

4 Conclusions

Compared to traditional subsoilers, the multi-subsoiler configurations and DEM-driven insights in this study present a more energy-efficient, soil-friendly, and technologically advanced solution for subsoiling. To investigate the actual tillage performance, the field experiments of six kinds of subsoilers with different types and space arrangements were carried out at a speed of 3 km/h under different space arrangements in the sowing season in an experimental field of 1 hm^2 with black soil. The choice of subsoiler type and its space arrangement showed a clear impact on soil disruption, fuel consumption, and mechanical resistance. The subsoiler had the least resistance at 600 mm spacing, compared with that of 500 mm and 700 mm. Additionally, with different spacings, the forces of TC-SM, TA-SM, and TDW-SM were smaller than those of TC-SC, TA-SC, and TDW-SC, which shows that the influence of the tine on force was greater than that of the shank. Mechanism of resistance with different tine and shank was analyzed, showing that the total tillage resistance was in proportion to the area of soil acting on the tine, tine width, and $\cos^2\lambda$, that is, $F_{\text{TDW-SC}}>F_{\text{TA-SC}}>F_{\text{TC-SC}}>F_{\text{TDW-SM}}>F_{\text{TA-SM}}>F_{\text{TC-SM}}$, which was consistent with the field test. The influences of TC-SM and TA-SM on tillage resistance with DEM were discussed, and were less than those of the field experiment, with an error of less than 10%. This is because the crop roots, straw residue, stones, or blunt subsoiler tines and shanks were not considered in simulation. Therefore, the tillage resistance in the simulation in DEM was smaller than that in the field, which is relatively reasonable and credible. The effect of spacing on soil disturbance behavior indicates that a mixed soil structure, with moderate soil disturbance and soil porosity ratio, and a spacing of 600 mm would be a good choice. These features highlight the novelty and significant advancement of this study compared to existing technologies.

Acknowledgements

This research was supported by Zhejiang Provincial Natural Science Foundation of China (Grant No. LQ23E050007), Huzhou Key Research and Development Project (Grant No. 2022ZD2068), Huzhou Science and Technology Special Commissioner Project (Grant No. 2023KT75), and National Key R&D Program of China (Grant No. 2022YFD1500600).

[References]

[1] Liu Z, Cao S L, Sun Z H, Wang H Y, Qu S D, Lei N, et al. Tillage effects on soil properties and crop yield after land reclamation. Scientific Reports, 2021; 11(1): 4611.

[2] Araya S N, Mitchell J P, Hopmans J W, Ghezzehei T A. Long-term impact of cover crop and reduced disturbance tillage on soil pore size distribution and soil water storage. Soil, 2022; 8(1): 177–198.

[3] Adil M, Zhang C, Yao Z J, Lu S Q, Qin Z Y, Wang J C, et al. Interactive effects of intercropping and mulching under conservation tillage as sustainable agriculture increased cotton productivity. Frontiers in Ecology and Evolution, 2023; 10: 1092636.

[4] Zabihi R, Mowla D, Karami H R. Artificial intelligence approach to predict drag reduction in crude oil pipelines. Journal of Petroleum Science and Engineering, 2019; 178: 586–593.

[5] Liu J A, Wang X L, Li H W, He J, Wang Q J, Li W Y. Optimization of structural parameters of subsoiler based on soil disturbance and traction resistance. Transactions of the CSAM, 2017; 48(2): 60–67.

[6] Plessis A D, Broeckhoven C, Yadroitsava I, Yadroitsev I, Hands C H, Kunjuet R, et al. Beautiful and functional: a review of biomimetic design in additive manufacturing. Additive Manufacturing, 2019; 27: 408–427.

[7] Plessis A D, Broeckhoven C. Looking deep into nature: a review of micro-computed tomography in biomimicry. Acta Biomaterialia, 2019; 85: 27–40.

[8] Hassanalian M, Abdelmoula H, Mohammadi S, Bakhtiyarov S, Goerlich J, Javedet U, et al. Aquatic animal colors and skin temperature: Biology's selection for reducing oceanic dolphin's skin friction drag. Journal of Thermal Biology, 2019; 84: 292–310.

[9] Qin K, Zhao Y, Zhang Y Z, Cao C M, Shen Z G. Lateral stress and its transmission law caused by operation of a double-wing subsoiler in sandy loam soil. Frontiers in Environmental Science, 2022; 10: 986361.

[10] Wang Y M, Lu C J, Chen J, Cui C H, Pan Y J, Pfleging W, et al. Effects of self-healing biomimetic subsoiler on tillage resistance, wear-corrosion performance and soil disturbance morphology under different soil types. Int J Agric & Biol Eng, 2023; 16(3): 7–14.

[11] Makange N R, Ji C Y, Nyalala I, Sunusi I I, Opiyo S. Prediction of precise subsoiling based on analytical method, discrete element simulation and experimental data from soil bin. Scientific Reports, 2021; 11: 11082.

[12] Wang Y M, Li N, Ma Y H, Tong J, Pfleging W, Sun J Y. Field experiments evaluating a biomimetic shark-inspired (BioS) subsoiler for tillage resistance reduction. Soil and Tillage Research, 2020; 196: 104432.

[13] Wang Y M, Xue W L, Ma Y H, Tong J, Liu X P, Sun J Y. DEM and soil bin study on a biomimetic disc furrow opener. Computers and Electronics in Agriculture, 2019; 156: 209–216.

[14] Huang Y X, Hang C G, Yuan M C, Wang B T, Zhu R X. Discrete element simulation and experiment on disturbance behavior of subsoiling. Transactions of the CSAM, 2016; 47(7): 80–88.

[15] Wang X Z, Yue B, Gao X J, Zheng Z Q, Zhu R X, Huang Y X. Discrete element simulations and experiments of disturbance behavior as affected by mounting height of subsoiler's wing. Transactions of the CSAM, 2018; 49(10): 124–136.

[16] Hang C G, Gao X J, Yuan M C, Huang Y X, Zhu R X. Discrete element simulations and experiments of soil disturbance as affected by the tine spacing of subsoiler. Biosystems Engineering, 2018; 168: 73–82.

[17] Shi Y Y, Jiang Y, Wang X C, Yu H M, Liu H, Chen J B. Innovation of strip fertilization planting for rice straw crushing with back-throwing and interrow-laying. Plant Methods, 2022; 18: 31.

[18] Ahmadi I. Effect of soil, machine, and working state parameters on the required draft force of a subsoiler using a theoretical draft-calculating model. Soil Research, 2016; 55(4): 389–400.

[19] Zhang X Y, Zhang L X, Hu X, Wang H, Shi X B. Calibrating contact parameters of typical rotary tillage components cutting soil based on different simulation methods. Scientific Reports, 2023; 13: 5757.

[20] Wang Y J, Wu, Y X, Cao C Y, Hen S, Zhao W S, Li Q S, et al. Effects of fertilizer reduction coupled with straw returning on soil fertility, wheat root endophytic bacteria, and the occurrence of wheat crown rot. Frontiers in Microbiology, 2023; 14: 1143480.